Title

Rotator cuff tendon assessment using magic-angle insensitive 3D ultrashort echo time cones magnetization transfer (UTE-Cones-MT) imaging and modeling with histological correlation

Journal

Journal of Magnetic Resonance Imaging, 48(1)

ISSN

1053-1807

Authors

Zhu, Yanchun
Cheng, Xin
Ma, Yajun
et al.

Publication Date

2018-07-01

DOI

10.1002/jmri.25914

Rotator Cuff Tendon Assessment Using Magic-Angle Insensitive 3D Ultrashort Echo Time Cones Magnetization Transfer (UTE-Cones-MT) Imaging and Modeling With Histological Correlation

Yanchun Zhu, PhD,[1,2] Xin Cheng, MD,[1,3] Yajun Ma, PhD,[1,4] Jonathan H. Wong, BS,[1,4] Yaoqin Xie, PhD,[2] Jiang Du, PhD,[1] and Eric Y. Chang, MD[4]*

Background: Rotator cuff tendons (RCTs) are challenging to image due to the "magic angle effect" and their short T_2.
Purpose: To assess the degree of magic angle sensitivity of human RCTs and to utilize a 3D ultrashort echo time Cones sequence with magnetization transfer preparation (UTE-Cones-MT) and two-pool quantitative MT modeling with histological correlation. We hypothesized that MT parameters would be less sensitive to the magic angle compared with conventional T_2 measurements.
Study Type: Prospective imaging pathologic correlation.
Specimen: Twenty cadaveric rotator cuff tendons were imaged at five sample orientations ranging from 0–90° relative to the B_0 field.
Field Strength/Sequence: 3T/3D UTE-Cones-MT and Carr–Purcell–Meiboom–Gill (CPMG).
Assessment: Two-pool quantitative MT modeling parameters and T_2 values were calculated in regions of interest drawn by a medical physicist. Histopathological analysis was performed and mild and severe tendinopathy groups were assigned by a histopathologist and histotechnician.
Statistical Tests: Coefficients of variations (CVs) were calculated for measures between the different orientations and group means were compared for each measure.
Results: CVs of T_2 and macromolecular fractions between orientations were 26.14 ± 16.82% and 6.18 ± 2.77% (mean ± SD), respectively. T_2 measurements at 0°, 27°, 70°, and 90° showed significant differences between the two histological groups ($P = 0.004$, 0.008, 0.003, and 0.015, respectively), but not at 55° ($P = 0.611$). Mean T_2 value ranges between orientations for the mild and severe tendinopathy groups were 15.27–30.32 msec and 20.81–35.85 msec, respectively, showing overlap despite statistically significant differences ($P = 0.003$). Macromolecular fractions at all angles showed significant differences between the two groups ($P < 0.0001$). Mean fraction ranges between orientations for the mild and severe tendinopathy groups were 14.32–17.17% and 10.00–13.75% respectively ($P < 0.0001$) with no overlap.
Data Conclusion: Compared with T_2, macromolecular fraction obtained with the 3D UTE-Cones-MT technique is resistant to the magic angle effect and is more sensitive to RCT degeneration.
Level of Evidence: 1
Technical Efficacy: Stage 2

J. MAGN. RESON. IMAGING 2017;00:000–000.

The rotator cuff tendon (RCT) is the primary dynamic stabilizer of the glenohumeral joint.[1] RCT pathology is common, and is present in up to 70% of cases that seek medical attention for shoulder pain.[2] Magnetic resonance imaging (MRI) is widely considered the gold standard for noninvasive evaluation of RCT tearing, but studies have shown low performance for the assessment of RCT tissue quality. For instance, using conventional MRI techniques,

View this article online at wileyonlinelibrary.com. DOI: 10.1002/jmri.25914

Received Oct 6, 2017, Accepted for publication Nov 16, 2017.

*Address reprint requests to: E.Y.C., VA San Diego Healthcare System, San Diego, CA 92161. E-mail: ericchangmd@gmail.com

From the [1]Department of Radiology, University of California, San Diego Medical Center, San Diego, California, USA; [2]Shenzhen Institute of Advanced Technology, Chinese Academic of Science, Shenzhen, China; [3]Department of Histology and Embryology, Jinan University School of Medicine, Guangzhou, China; and [4]Radiology Service, VA San Diego Healthcare System, San Diego, California, USA.

sensitivity for tendinosis ranges from 13–79% and there is exceedingly poor interobserver reliability.[3,4] Unfortunately, this represents an unmet need, since tissue quality affects clinical decision making and plays a central role in the likelihood of RCT healing after surgical repair.[3]

Two critical barriers to the use of MRI for assessment of tendon tissue quality include the confounding factor of the "magic angle effect" and the short T_2 of tendons. Magic angle effect is seen in collagen-rich tissues and is due to unaveraged dipolar interactions of proton nuclear spins.[5] As the tissue fiber orientation approaches 54.7° relative to the main magnetic field, frequency changes from dipolar interactions are minimized and signal intensity is maximum.[6] This may be less of an issue for tendons with a more constant orientation in clinical imaging, such as the Achilles tendon, but the RCT orientation is varied and likely consistently courses through the magic angle. A previous study has reported up to a 6-fold change in signal intensity of histologically normal RCT at 3T purely due to different orientations of the shoulder.[7] Such large signal intensity changes may exceed those produced by disease.

Another challenge with imaging of tendons is due to their composition and structure, which results in a very short T_2. In particular, the portions of RCT where fascicles tend to be oriented parallel or perpendicular to the main magnetic field have short T_2s, and are often seen as hypointense when imaged with conventional clinical sequences.[6,7] The low signal-to-noise ratio of these portions of tendon might preclude differentiation of healthy tendon versus fibrotic tissue.

Ultrashort echo time (UTE) MRI sequences are one solution to this problem by permitting signal detection before decay to background levels.[8] More recently, the UTE magnetization transfer (UTE-MT) technique with two-pool modeling was implemented on cadaveric Achilles tendons.[9] The UTE-MT technique relies on the phenomenon of magnetization exchange between directly detected water protons (both free and restricted) and macromolecular protons, with transverse relaxations too short to directly image even with UTE sequences. Signal model fitting provides multiple parameters, including water and macromolecular proton fractions, as well as relaxation and exchange rates.[10] UTE-MT has demonstrated promise as a clinically compatible quantitative technique that is resistant to the magic angle effect.[9] However, the degree of magic angle sensitivity of the RCT has not been systematically studied and quantitative MT techniques have not yet been employed on RCT. Furthermore, it is currently unclear how sensitive MT parameters are to pathology.

The purpose of this study was to assess the degree of magic angle sensitivity of human RCT and to utilize the 3D UTE Cones sequence with magnetization transfer preparation (UTE-Cones-MT) and two-pool quantitative MT modeling with histological correlation.

Materials and Methods

Sample Preparation

This prospective study was approved by our Institutional Review Board with a waiver of informed consent for cadaveric specimen work. Written, informed consent was obtained from all living participants prior to examination. For this project, 20 RCTs were harvested from 10 donor shoulders (five females, five males; mean age 86 years old). Specimens had undergone a single freeze–thaw cycle prior to dissection and subsequent imaging. A deltopectoral approach was used to expose the superior portion of the rotator cuff. No full-thickness cuff tears were appreciated at the time of dissection in nine of the shoulders. In these cases, the supraspinatus and infraspinatus tendons were removed by cutting at the myotendinous junction and sharply dissecting the tendon from the greater tuberosity. In one shoulder, a massive superior cuff tear was present with retraction to the glenoid margin, and the scarred supraspinatus and infraspinatus tendons were removed. On average, tendon specimens measured ~4.5 cm in length, as shown in Fig. 1A. Tendons were placed in a sealed container with Fomblin to minimize dehydration and susceptibility artifact.[11]

MRI Protocol

Imaging was performed with a 3T clinical MRI scanner (Signa Twinspeed, GE Healthcare, Milwaukee, WI) with a maximum gradient strength of 40 mT/m and a maximum slew rate of 150 mT/m/ms. A birdcage extremity coil (BC-10, Medspira, Minneapolis, MN) was used for signal excitation and reception. The 3D UTE-Cones-MT sequence employed an MT preparation followed by multiple 3D UTE-Cones interleaves to accelerate data acquisition.[10] Specifically, this sequence uses a unique *k*-space trajectory that samples data along evenly spaced twisting paths in the shape of multiple cones.[12–14] The MT preparation consisted of a Fermi shaped radiofrequency (RF) pulse (duration = 8 msec, bandwidth = 160 Hz) followed by a gradient crusher. The 3D UTE-MT imaging parameters include: repetition time (TR) = 100 msec, echo time (TE) = 32 μs, flip angle (FA) = 7°, bandwidth (BW) = ±62.5 kHz, field of view (FOV) = 8 cm, reconstruction matrix = 128 × 128, slice thickness = 3 mm, slice number = 10–12; nine interleaves per MT preparation pulse, three MT powers (300°/550°/750°), and five MT frequency offsets (2/5/10/20/50 kHz), with a total of 15 different MT datasets, and a total scan time of ~10 minutes. T_1 was measured with the 3D UTE-Cones acquisition with the same plane and spatial resolution and other imaging parameters including: TRs = 5.4/20/50/80/120 msec, TE = 32 μs, FA = 20°, BW = ±62.5 kHz. A multislice 2D Carr–Purcell–Meiboom–Gill (CPMG) sequence was used for T_2 measurement with imaging parameters including: TR = 800 msec, TEs = 7.9/15.8/23.7/31.6/39.5/47.4/55.3/63.2 msec, FOV = 8 cm, acquisition matrix = 256 × 192, slice thickness = 3 mm, slice space = 0.6 mm, BW = ±32.5 kHz. The same protocol was applied to each RCT five times, with the long-axis of the tendons oriented 0°, 27°, 55°, 70°, and 90° relative to the B_0 field.

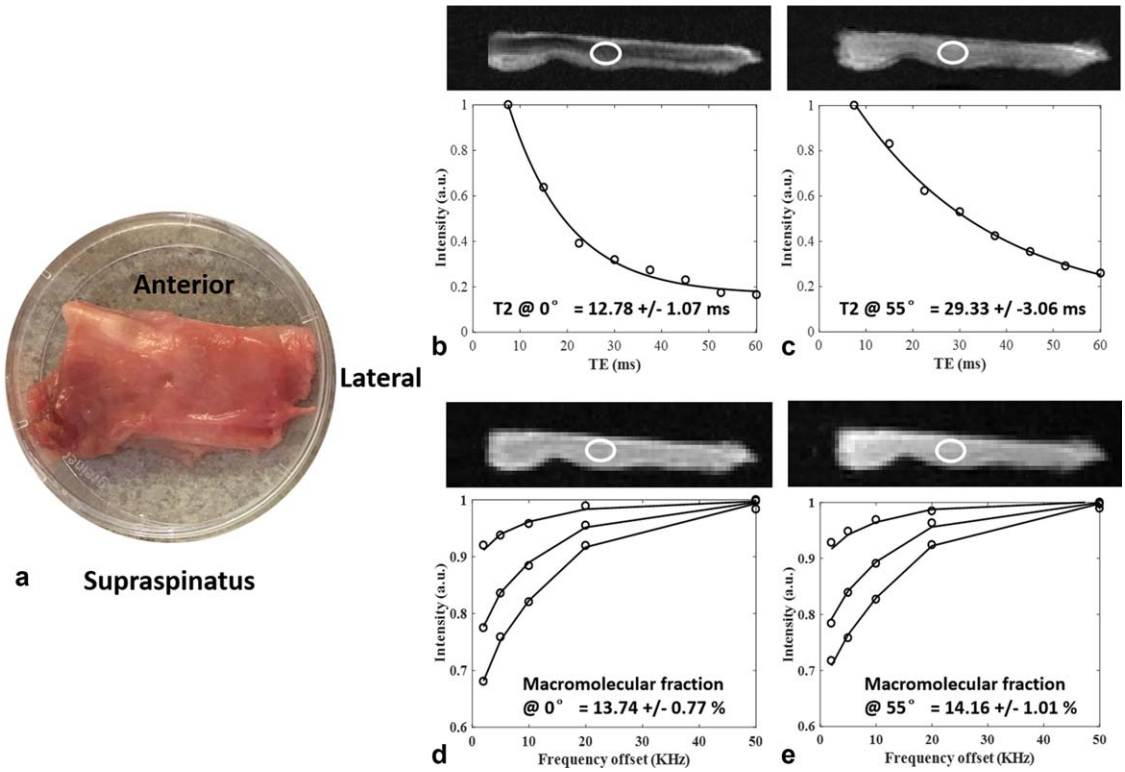

FIGURE 1: Supraspinatus tendon from an 87-year-old. (a) Tendon as viewed from the bursal side, cut from the myotendinous junction to the footprint. Spin-echo images with T_2 curves at (b) 0° and (c) 55° demonstrates marked signal intensity change and a 129% increase in T_2 between the two orientations. UTE-Cones-MT images with two-pool modeling curves at (d) 0° and (e) 55° demonstrates stable high signal and a 3% difference in macromolecular fraction between the two orientations.

In Vivo MRI Protocol

To demonstrate in vivo feasibility, the 3D UTE-Cones-MT sequence was applied to three healthy volunteers (three males; 34.0 ± 4.6 years, mean ± standard deviation [SD]). A three-channel shoulder coil was used for signal reception. The 3D UTE-Cones-MT sequence was acquired in the coronal oblique plane with imaging parameters including: TR = 100 msec, TE = 32 μs, FA = 7°, BW = ± 62.5 kHz, FOV = 17 cm, reconstruction matrix = 256 × 256, slice thickness = 3 mm, slice number = 20; 11 interleaves per MT preparation pulse, three MT powers (300°/550°/750°), and five MT frequency offsets (2/5/10/20/50 kHz), with a total of 15 different MT datasets, and a total scan time of 15 minutes. T_1 was measured with the 3D UTE-Cones acquisition with the same plane, spatial resolution, and other imaging parameters including: TR = 20, TE = 32 μs, FA = 5/10/20/30°, BW = ±62.5 kHz, with a total scan time of ~5 minutes. In addition, a 3D dual-TR UTE-Cones sequence was also used for actual flip angle imaging similar to that previously described[15] in order to correct for B_1 inhomogeneity as a result of off-isocenter imaging, with a total scan time of ~5 minutes.

MRI Analysis

Analysis was performed using MatLab (MathWorks, 2016b, Natick, MA) on the Digital Imaging and Communications in Medicine (DICOM) images obtained by the protocols described above. Rigid body linear image registration was performed using the Functional MRI of the Brain (FMRIB) Linear Image Registration Tool among different angle orientations to ensure that the same anatomic location was compared.[16,17] Regions of interest (ROIs) were drawn using the UTE-Cones images without MT preparation with an average of 30 pixels per ROI (Y.Z., who was blinded to the histology results). UTE-Cones images were used to minimize selection bias since the images demonstrated a relatively uniform appearance. ROIs for T_2 measurements were adjusted based on matrix sizes of CPMG and T_1 images with an average of 60 pixels per ROI. In cases where the ROIs were found by the senior author (E.Y.C.) to encompass regions that were extremely heterogeneous on histology (eg, locations where a confident histology score could not be assigned), the ROIs were redrawn.

A Levenberg–Marquardt algorithm was employed for the nonlinear least-squares fitting in MT modeling, as well as T_1 and T_2 fitting. Two-pool UTE-Cones-MT modeling and parameter mapping were performed on the datasets using previously described methods.[9,10] ROI analyses were performed and mean and standard deviation of T_2 relaxation and macromolecular proton fractions were calculated.

Histologic Preparation and Analysis

After MRI protocols were fully completed, tendons were fixed in 10% zinc formalin, dehydrated with alcohol, and embedded in paraffin. The 7-μm sections were cut and stained with hematoxylin and eosin (H&E). On average, 30 slides were made per RCT specimen, sampling various regions of each tendon. The senior author (E.Y.C.) located the slides corresponding to the ROIs drawn on MRI and a pathologist (X.C., 19 years of experience in histopathology) and histotechnician (J.H.W., 16 years of experience in histopathology), who were both blinded to the MRI results,

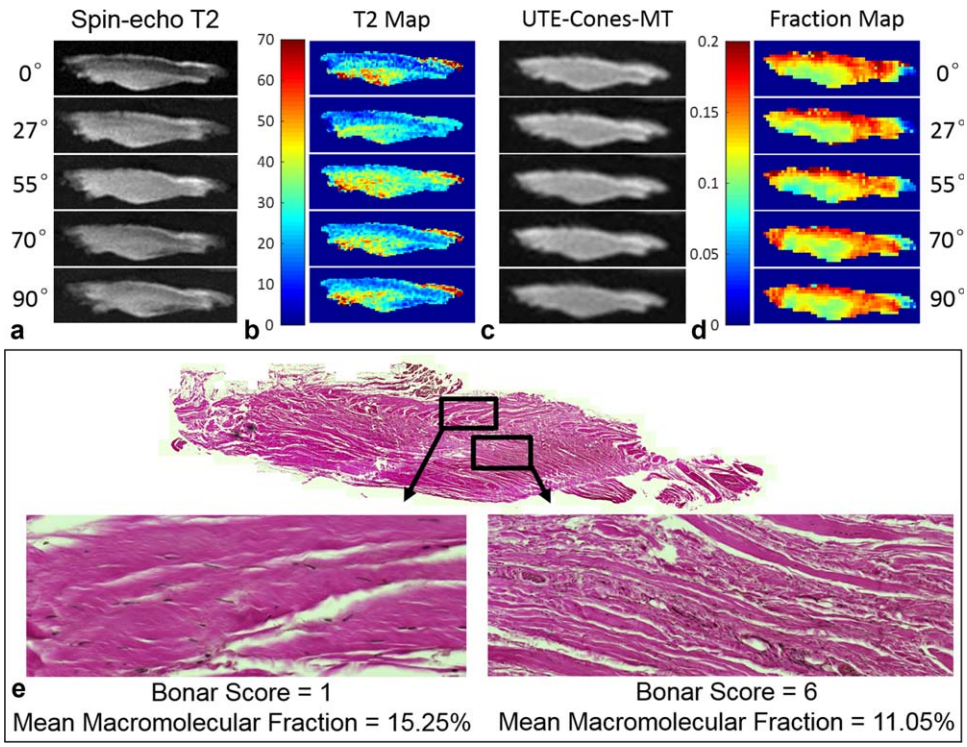

FIGURE 2: Infraspinatus tendon from an 81-year-old. (a) Spin-echo and (b) T_2 pixel maps between orientations demonstrate tremendous variability in signal and T_2 values, respectively. (c) UTE-Cones-MT and (d) macromolecular fraction pixel maps between orientations are stable, but the pixel maps demonstrate spatial heterogeneity. (e) H&E staining slide demonstrates mild tendinopathy at an ROI along the bursal surface with total Bonar Score of 1 (normal cells and vascularity with scores of 0 and mild collagen disruption with score of 1) with mean macromolecular fraction of 15.25%, whereas an ROI in the intrasubstance shows severe tendinopathy with Bonar Score of 6 (increased incidence of abnormally rounded cells, moderately abnormal collagen, and increased vascularity with scores of 2 for each) with mean macromolecular fraction of 11.05%.

independently applied a modified Bonar score.[18] Specifically, tendons were evaluated for changes in tenocyte morphologic characteristics, collagen bundle characteristics, and variations in vascularity, with scores in each category ranging from 0 to 3. Two groups were assigned, defined as those with mild tendinopathy (Bonar score <3) or with severe tendinopathy (Bonar score ≥3).[19] After the provided slides corresponding to the MRI ROIs were scored, all histology slides were qualitatively assessed.

Statistical Analysis

Statistical analyses were performed using the SPSS software package (v. 21; SPSS, Chicago, IL). The Shapiro–Wilk test was used to assess normality. Two-way mixed intraclass correlation (ICC) coefficients were used to assess interrater reliability for determination of Bonar scores. (ICC <0.40, poor agreement; ≥0.40 and <0.60, moderate agreement; ≥0.60 and <0.80, substantial agreement; and ≥0.80, excellent agreement).[20] Descriptive statistics were performed and coefficient of variations (CVs, representing the ratio of standard deviation to the mean) were calculated for MRI measures between the different orientations. Student's *t*-test was performed to compare means of each MRI measure for the Bonar <3 and Bonar ≥3 groups. $P < 0.05$ was considered to represent significant findings.

Results

All RCTs were heterogeneous in appearance on both MRI pixel maps and when assessed histologically. For the ROI analyses, seven demonstrated mild tendinopathy (Bonar scores <3), with the rest demonstrating severe tendinopathy (Bonar scores ≥3). ICC coefficient for Bonar scores between the two readers was 0.89 ($P < 0.0001$), indicating excellent agreement. Using binarized categories of Bonar scores <3 or ≥3, histology readers agreed perfectly on all cases.

A representative RCT sample is shown in Fig. 1, with results of both T_2 fitting and UTE-Cones-MT modeling for the supraspinatus tendon oriented at 0° and 55°. Tendon signal intensity varied tremendously on CPMG images between angles and this was reflected by a vast variation of T_2 values, which for the ROI demonstrated, increased from 12.78 msec at 0° to 29.33 msec at 55° (129% increase). The UTE-Cones-MT images demonstrated abundant signal on all orientations with resultant excellent fitting (residuals between 0.5–0.6%). The macromolecular fraction remains relatively constant from 13.74% at 0° to 14.16% at 55°, representing a 3% difference.

Figure 2 shows a supraspinatus tendon sample from an 81-year-old woman. Both T_2 and macromolecular fraction pixel maps are heterogeneous. Magic angle effects complicate the interpretation of T_2 pixel maps, whereas the macromolecular fraction demonstrates very little variability between angles. ROI analysis in an area with less degeneration at the bursal side shows a lower mean T_2 value

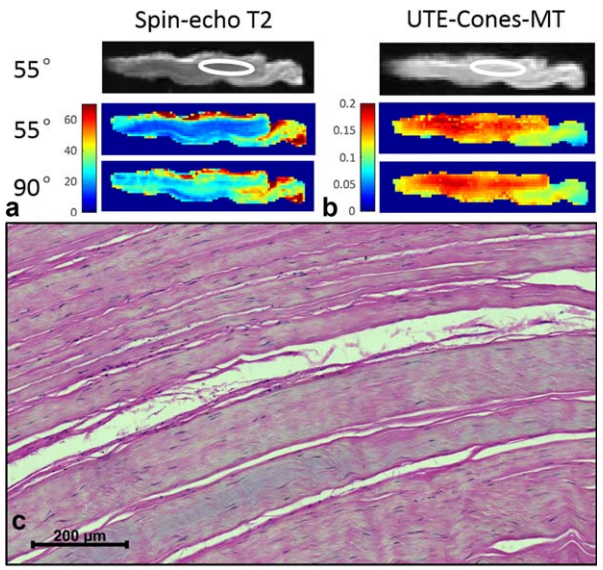

FIGURE 3: Infraspinatus tendon ROI that was histologically normal. (a) Sample spin-echo image and T_2 pixel maps at 55° and 90° demonstrate tremendous variability in T_2 values between orientations. For the ROI shown, T_2 values ranged from 12.24–29.44 msec, with a 141% change between the two orientations. (b) Sample UTE-Cones-MT image with macromolecular fraction pixel maps at 55° and 90° show stable values between orientations. For the ROI shown, macromolecular fractions ranged from 16.29–17.16%, representing a 5% change between orientations. (c) H&E slide demonstrates a total Bonar Score of 0 (normal cells, collagen, and vascularity).

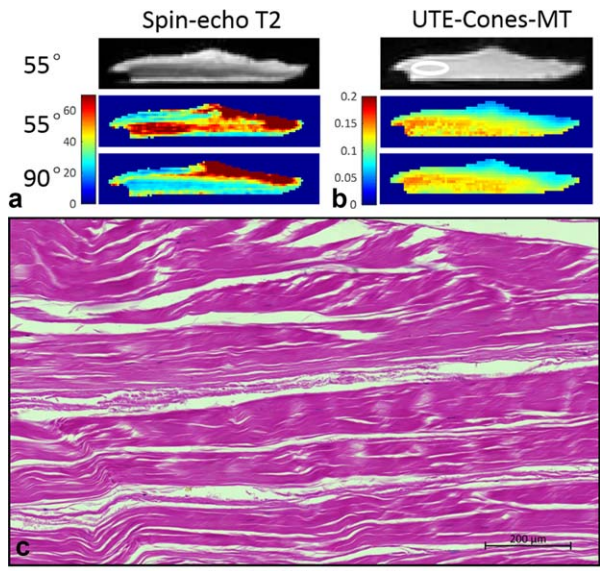

FIGURE 4: Infraspinatus tendon ROI with mild tendinosis. (a) Sample spin-echo image and T_2 pixel maps at 55° and 90° demonstrate tremendous variability in T_2 values between orientations. For the ROI shown, T_2 values ranged from 17.09–68.19 msec, representing a 299% change between the two orientations. (b) Sample UTE-Cones-MT image with macromolecular fraction pixel maps at 55° and 90° show stable values between orientations. For the ROI shown, macromolecular fractions ranged from 14.16–15.08%, representing a 6% change between orientations. (c) H&E-stained slide demonstrates a total Bonar Score of 1 (normal cells and collagen with scores of 0 and mildly abnormal vascularity with score of 1).

compared with an area with more degeneration in the intrasubstance region (35.85 msec vs. 22.14 msec, respectively). However, there was a large range of values at individual angles (29.85–42.58 msec vs. 19.75–29.40 msec, respectively). Mean macromolecular fractions were higher in regions of less degeneration (15.25% vs. 11.05%). Of note, however, the range of values at individual angles was narrow and the values between groups were well separated (14.38–16.05% vs. 10.58–11.42%).

A sample with an ROI that was histologically normal (Bonar score 0) is shown in Fig. 3. Mean T_2 value was 19.83 msec, but a range of 12.24–29.44 msec was seen, representing a 141% change between orientations. Mean macromolecular fraction was 16.68% with a range of 16.29–17.16%, representing a 5% change between orientations. Another sample with minimal degeneration is shown in Fig. 4. Mean T_2 value was 30.32 msec with a range of 17.09–68.19 msec, representing a 299% change between orientations. Mean macromolecular fraction was 14.76% with a range of 14.16–15.08%, representing a 6% change between orientations.

One of the samples with the highest Bonar scores is shown in Fig. 5. Mean T_2 value was 33.36 msec, with a range of 31.25–34.80 msec, representing an 11% change between orientations. Mean macromolecular fraction was 10.88%, with a range of 10.08–11.74%, representing a 16% change between orientations. Less orientation dependence of T_2 was present in the severely degenerated samples. As Figs. 3–5 show, mean T_2 values increase in trend with degeneration; however, the range of values between orientations demonstrate considerable overlap. In contrast, the range of values for the macromolecular fractions demonstrate little to no overlap.

Bar graphs with 95% confidence intervals are shown in Fig. 6, illustrating several overlapping mean T_2 values when orientations are compared between groups. Specifically, for mean T_2 values, a range of 15.27–30.32 msec was seen for the mild tendinopathy group and a range of 20.81–35.85 msec was seen for the severe tendinopathy group. On the other hand, no overlap was seen for the mean macromolecular fractions, with a range of 14.32–17.17% for the mild tendinopathy group and 10.00–13.75% for the severe tendinopathy group.

For all samples, mean CV of T_2 values between orientations was 26.14 ± 16.82% (mean ± SD) and mean CV of macromolecular fraction was 6.18 ± 2.77% (mean ± SD). Mean T_2 and macromolecular fractions for tendon groups with mild tendinopathy (Bonar <3) versus severe tendinopathy (Bonar ≥ 3) are shown in Tables 1 and 2,

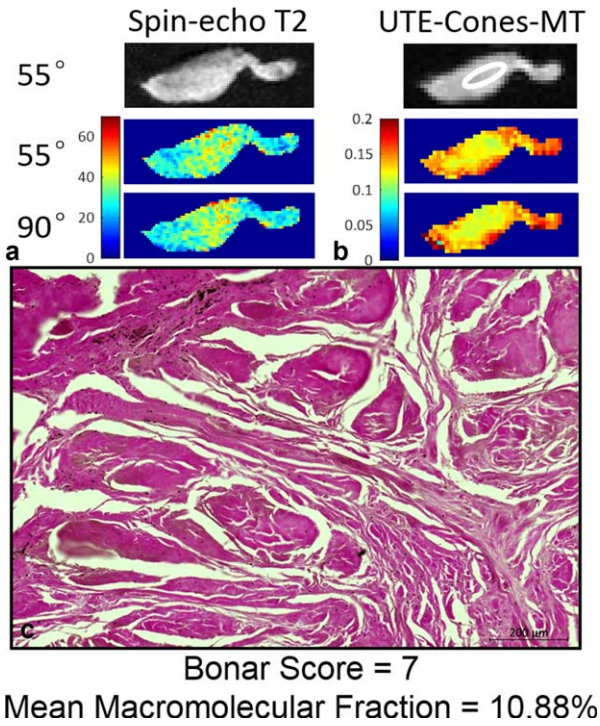

FIGURE 5: Infraspinatus tendon ROI with severe tendinosis. (a) Sample spin-echo image and T_2 pixel maps at 55° and 90° demonstrate little variability in signal and T_2 values between orientations, indicative of little anisotropy. For the ROI shown, T_2 values ranged from 31.25–34.80 msec, with an 11% change between the two orientations. (b) Sample UTE-Cones-MT image with macromolecular fraction pixel maps at 55° and 90° show stable values between orientations. For the ROI shown, macromolecular fractions ranged from 10.08–11.74%, representing a 16% change between orientations. (c) H&E-stained slide demonstrates Bonar Score of 7 (abnormal cells with a score of 2, disrupted collagen with a score of 2, and high vascularity with a score of 3).

respectively. Using T_2 measurements, four of the five angles (0°, 27°, 70°, and 90°) and the mean value of all angles showed significant differences between the two groups (Table 1). Using macromolecular fractions, all angles and the mean value of all angles showed significant differences between the two groups (Table 2).

In vivo feasibility was demonstrated on the three healthy volunteers, yielding high-quality images with minimal artifacts (Fig. 7). ROI analysis of the distal supraspinatus tendons near the critical zone of Codman showed excellent fitting curves, with a macromolecular fraction of 14.47 ± 0.27 (mean ± SD).

Discussion

In this study we utilized the 3D UTE-Cones-MT sequence with two-pool MT modeling on cadaveric RCTs. Our results demonstrate that macromolecular fractions are more resistant to the magic angle effect compared with T_2 relaxation measurements and demonstrate higher performance for distinguishing between degrees of tendinopathy. Hodgson et al previously used a 2D version of the technique to assess the Achilles tendons of eight healthy volunteers and one patient with psoriatic arthritis. They similarly found that the clinically pathologic tendon demonstrated a lower macromolecular fraction than all eight volunteers.[21] Ma et al also previously used the 2D UTE-MT technique on Achilles tendons and found minimal angular dependence with mean macromolecular fractions ranging from 19.6–20.0%.[9] Ma et al also recently used a 3D UTE-Cones-MT technique on cortical bone samples and showed mean macromolecular fractions of 59.4%.[10] Our results demonstrate that a lower range of macromolecular fractions are expected from the unique RCT in comparison to the Achilles tendon or cortical bone. Furthermore, our results suggest that a lower macromolecular fraction appears to be associated with worse tissue degeneration.

T_2 values are sensitive to water and macromolecular content, and differences in relaxation times have long been used to differentiate between normal and abnormal tissues. However, in collagen-rich anisotropic tissues, T_2 values are

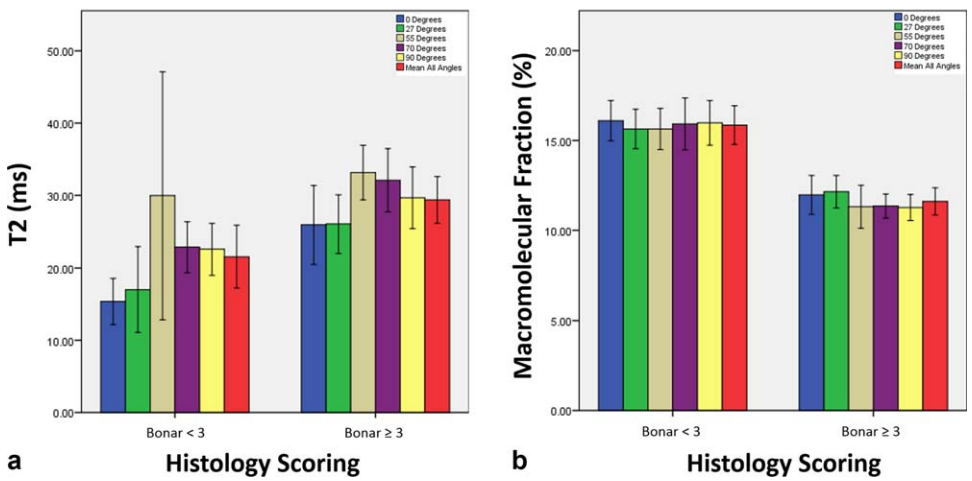

FIGURE 6: Bar graphs demonstrating (a) T_2 values and (b) mean macromolecular fractions with 95% confidence intervals for mild and severe tendinopathy groups.

TABLE 1. Comparison of T2 Values Between Mild and Severe Tendinopathy Groups for Various Orientations

Histology	T2 (msec)						
	0°	27°	55°	70°	90°	Mean all angles	Coefficient of variation (%)
Bonar <3	15.37 ± 3.46	17.00 ± 6.38	29.97 ± 18.53	22.84 ± 3.78	22.54 ± 3.86	21.54 ± 4.67	37.51 ± 17.79
Bonar ≥3	25.92 ± 7.60	26.04 ± 5.64	33.15 ± 5.28	32.09 ± 6.13	29.66 ± 5.97	29.37 ± 4.54	18.18 ± 10.99
P-value	**0.004**	**0.008**	0.611	**0.003**	**0.015**	**0.003**	

TABLE 2. Comparison of Macromolecular Fractions Between Mild and Severe Tendinopathy Groups for Various Orientations

Histology	Macromolecular fraction (%)						
	0°	27°	55°	70°	90°	Mean all angles	Coefficient of variation (%)
Bonar <3	16.10 ± 1.21	15.64 ± 1.19	15.64 ± 1.24	15.92 ± 1.56	15.98 ± 1.34	15.86 ± 1.16	4.09 ± 1.90
Bonar ≥3	11.97 ± 1.51	12.15 ± 1.27	11.32 ± 1.67	11.35 ± 0.93	11.27 ± 1.01	11.61 ± 1.06	7.64 ± 2.34
P-value	**<0.0001**	**<0.0001**	**<0.0001**	**<0.0001**	**<0.0001**	**<0.0001**	

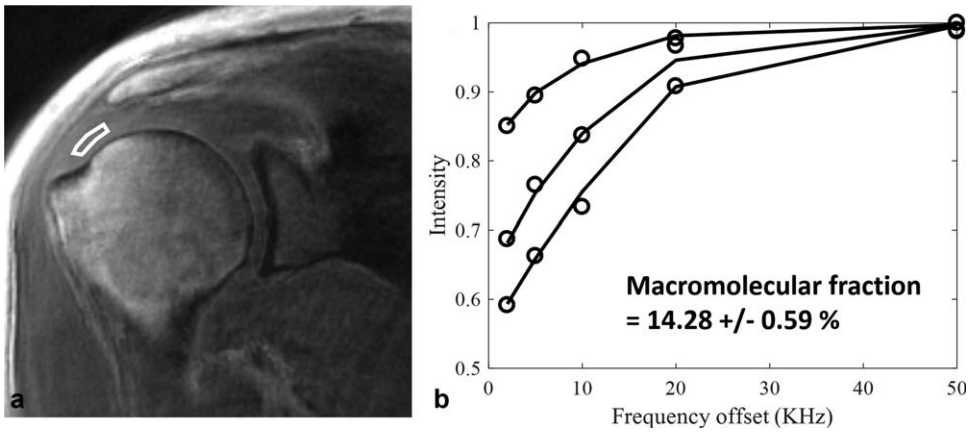

FIGURE 7: UTE-Cones-MT sequence in an asymptomatic 38-year-old volunteer. (a) Coronal oblique UTE-Cones-MT image demonstrates high quality and the region of interest which was used for quantification. (b) Fitting curve from two-pool MT modeling shows excellent fit with mean macromolecular fraction of 14.28%.

exquisitely sensitive to orientation. In cartilage, Shao et al found that T_2 values can increase by 232% depending on orientation.[22] In Achilles tendon, Ma et al found up to a 6-fold increase in T_2* depending on orientation.[9] We have now shown similar changes in RCT with up to a 299% change in T_2 values depending on orientation. It is important to point out that anisotropy leads to variations in T_2 values, including both increases and decreases, depending on the reference orientation.[23–25] Spencer and Pleshko highlighted a fundamental limitation of T_2—specificity that a statistical significance of group means in a research setting does not necessarily translate into a clinically useful outcome measure for detection of disease on an individual level.[26] Utilizing a single T_2 relaxation value for differentiation between normal and abnormal cartilage leads to an estimated sensitivity of 82% and specificity of 84% when the highest quality data (acquired on a high-performance nuclear magnetic resonance spectrometer) is available.[26] Our results mirror this observation, whereby the range T_2 values of mild versus severely degenerated tendons overlapped for all angles, despite demonstrating statistical significance between means for 3 of 5 angles evaluated.

Few studies to date have utilized quantitative MRI on RCTs and, to the best of our knowledge, all have been measures of transverse relaxation time (T_2 or T_2*).[27–29] The T_2 values in our sample are within the range of those reported by Anz et al, who evaluated supraspinatus tendons in 30 asymptomatic volunteers and found mean T_2 values ranging from 30–40 msec, although large standard deviations were present.[27] Ganal et al evaluated 50 subjects (15 volunteers, 11 patients with tendinosis, and 24 patients with tears) and found statistically significant differences in 3 of 12 supraspinatus tendon regions when compared between groups.[28] Most tendon regions demonstrated tremendous overlap in T_2 values between groups, and even in those regions that demonstrated statistically significant differences, overlapping ranges were present, consistent with our findings.

Our study has several limitations. First, this was primarily a cadaveric study with a selection bias of elderly patients. While Anz et al did not find a relationship between T_2 values and age,[27] the relationship between age and MT parameters remains to be studied, and therefore caution should be exercised prior to extrapolation of our results to a younger population. Second, use of the Bonar score remains under debate. Fearon et al found that the extent of tendon degeneration as assessed by the Bonar score varied depending on the area that was graded.[30] Our study attempted to overcome this by utilizing ROIs that were more histologically homogenous, but this was not standardized. Third, relaxation times are temperature-dependent[31–33] and the RCTs in our experiments were imaged at room temperature. In particular, T_1 would be expected to increase from room temperature to body temperature. However, preliminary results from our healthy volunteers suggest that macromolecular fractions between specimens and in vivo are comparable. Fourth, the UTE-Cones-MT sequence is not yet commercially available. However, utilization of this sequence only requires software installation without hardware modifications. Of note, the UTE sequence has been successfully employed on MRI machines from every major vendor. Finally, our UTE-Cones-MT imaging parameters were not optimized for the in vivo condition, since our study focused on cadaveric specimens. A number of acceleration techniques are possible, including lowering the total number of datasets (fewer powers and/or frequency offsets) from the 15 that were utilized in this study. In addition, 20 slices were obtained for each volunteer of this study; fewer slices would directly decrease imaging times. Utilization of advanced acceleration techniques such as parallel imaging or compressed sensing reconstruction[34] could further optimize imaging times, although the impact of this on quantification also remains to be studied.

In conclusion, we found that anisotropy has a large effect on T_2 values and a very small effect on

macromolecular fractions as obtained through the 3D UTE-Cones-MT technique. The large variability of T_2 values limits the ability of this measure for distinguishing between mild and severe tendinopathy as measured through histology. In comparison, the macromolecular fraction is able to be used to distinguish between mild and severe tendinopathy at all angles and the range of values between groups are better separated when compared with T_2.

Acknowledgment

Contract grant sponsor: VA Clinical Science Research and Development Service; contract grant number: Merit Award I01CX001388; Contract grant sponsor: National Institutes of Health (NIH); contract grant number: 1R01 AR062581; 1R01 AR068987; Contract grant sponsor: National Key Research Program of China; contract grant number: 2016YFC0105102; Contract grant sponsor: Union of Production, Study and Research Project of Guangdong Province; contract grant number: 2015B090901039; GE Healthcare.

References

1. Kramer EJ, Bodendorfer BM, Laron D, et al. Evaluation of cartilage degeneration in a rat model of rotator cuff tear arthropathy. J Shoulder Elbow Surg 2013;22:1702–1709.
2. Shanahan EM, Sladek R. Shoulder pain at the workplace. Best Pract Res Clin Rheumatol 2011;25:59–68.
3. Robertson PL, Schweitzer ME, Mitchell DG, et al. Rotator cuff disorders: interobserver and intraobserver variation in diagnosis with MR imaging. Radiology 1995;194:831–835.
4. Roy JS, Braen C, Leblond J, et al. Diagnostic accuracy of ultrasonography, MRI and MR arthrography in the characterisation of rotator cuff disorders: a systematic review and meta-analysis. Br J Sports Med 2015;49:1316–1328.
5. Berendsen HJC. Nuclear magnetic resonance study of collagen hydration. J Chem Phys 1962;36:3297.
6. Krasnosselskaia LV, Fullerton GD, Dodd SJ, Cameron IL. Water in tendon: orientational analysis of the free induction decay. Magn Reson Med 2005;54:280–288.
7. Chang EY, Szeverenyi NM, Statum S, Chung CB. Rotator cuff tendon ultrastructure assessment with reduced-orientation dipolar anisotropy fiber imaging. AJR Am J Roentgenol 2014;202:W376–378.
8. Chang EY, Du J, Chung CB. UTE imaging in the musculoskeletal system. J Magn Reson Imaging 2015;41:870–883.
9. Ma YJ, Shao H, Du J, Chang EY. Ultrashort echo time magnetization transfer (UTE-MT) imaging and modeling: magic angle independent biomarkers of tissue properties. NMR Biomed 2016;29:1546–1552.
10. Ma YJ, Chang EY, Carl M, Du J. Quantitative magnetization transfer ultrashort echo time imaging using a time-efficient 3D multispoke Cones sequence. Magn Reson Med 2017 [Epub ahead of print].
11. Chang EY, Du J, Bae WC, Statum S, Chung CB. Effects of Achilles tendon immersion in saline and perfluorochemicals on T2 and T2*. J Magn Reson Imaging 2014;40:496–500.
12. Carl M, Bydder GM, Du J. UTE imaging with simultaneous water and fat signal suppression using a time-efficient multispoke inversion recovery pulse sequence. Magn Reson Med 2016;76:577–582.
13. Gurney PT, Hargreaves BA, Nishimura DG. Design and analysis of a practical 3D cones trajectory. Magn Reson Med 2006;55:575–582.
14. Johnson KM. Hybrid radial-cones trajectory for accelerated MRI. Magn Reson Med 2017;77:1068–1081.
15. Yarnykh VL. Actual flip-angle imaging in the pulsed steady state: a method for rapid three-dimensional mapping of the transmitted radiofrequency field. Magn Reson Med 2007;57:192–200.
16. Jenkinson M, Smith S. A global optimisation method for robust affine registration of brain images. Med Image Anal 2001;5:143–156.
17. Jenkinson M, Bannister P, Brady M, Smith S. Improved optimization for the robust and accurate linear registration and motion correction of brain images. NeuroImage 2002;17:825–841.
18. Cook JL, Feller JA, Bonar SF, Khan KM. Abnormal tenocyte morphology is more prevalent than collagen disruption in asymptomatic athletes' patellar tendons. J Orthop Res 2004;22:334–338.
19. Cross JA, Cole BJ, Spatny KP, et al. Leukocyte-reduced platelet-rich plasma normalizes matrix metabolism in torn human rotator cuff tendons. Am J Sports Med 2015;43:2898–2906.
20. Altman DG. Practical statistics for medical research. Boca Raton, FL: Chapman & Hall/CRC: 1999.
21. Hodgson RJ, Evans R, Wright P, et al. Quantitative magnetization transfer ultrashort echo time imaging of the Achilles tendon. Magn Reson Med 2011;65:1372–1376.
22. Shao H, Pauli C, Li S, et al. Magic angle effect plays a major role in both T1rho and T2 relaxation in articular cartilage. Osteoarthritis Cartilage 2017 [Epub ahead of print].
23. Goodwin DW. MR imaging of the articular cartilage of the knee. Semin Musculoskelet Radiol 2009;13:326–339.
24. Markhardt BK, Chang EY. Hypointense signal lesions of the articular cartilage: a review of current concepts. Clin Imaging 2014;38:785–791.
25. Markhardt BK, Kijowski R. The clinical significance of dark cartilage lesions identified on MRI. AJR Am J Roentgenol 2015;205:1251–1259.
26. Spencer RG, Pleshko N. How do statistical differences in matrix-sensitive magnetic resonance outcomes translate into clinical assignment rules? J Am Acad Orthop Surg 2013;21:438–439.
27. Anz AW, Lucas EP, Fitzcharles EK, Surowiec RK, Millett PJ, Ho CP. MRI T2 mapping of the asymptomatic supraspinatus tendon by age and imaging plane using clinically relevant subregions. Eur J Radiol 2014;83:801–805.
28. Ganal E, Ho CP, Wilson KJ, et al. Quantitative MRI characterization of arthroscopically verified supraspinatus pathology: comparison of tendon tears, tendinosis and asymptomatic supraspinatus tendons with T2 mapping. Knee Surg Sports Traumatol Arthrosc 2016;24:2216–2224.
29. Krepkin K, Bruno M, Raya JG, Adler RS, Gyftopoulos S. Quantitative assessment of the supraspinatus tendon on MRI using T2/T2* mapping and shear-wave ultrasound elastography: a pilot study. Skeletal Radiol 2017;46:191–199.
30. Fearon A, Dahlstrom JE, Twin J, Cook J, Scott A. The Bonar score revisited: region of evaluation significantly influences the standardized assessment of tendon degeneration. J Sci Med Sport 2014;17:346–350.
31. Vesanen PT, Zevenhoven KC, Nieminen JO, Dabek J, Parkkonen LT, Ilmoniemi RJ. Temperature dependence of relaxation times and temperature mapping in ultra-low-field MRI. J Magn Reson 2013;235:50–57.
32. Birkl C, Langkammer C, Haybaeck J, et al. Temperature-induced changes of magnetic resonance relaxation times in the human brain: a postmortem study. Magn Reson Med 2014;71:1575–1580.
33. Han M, Rieke V, Scott SJ, et al. Quantifying temperature-dependent T1 changes in cortical bone using ultrashort echo-time MRI. Magn Reson Med 2015;74:1548–1555.
34. Lustig M, Donoho D, Pauly JM. Sparse MRI: The application of compressed sensing for rapid MR imaging. Magn Reson Med 2007;58:1182–1195.